Marine ice in Larsen Ice Shelf

Paul R. Holland,[1] Hugh F. J. Corr,[1] David G. Vaughan,[1] Adrian Jenkins,[1] and Pedro Skvarca[2]

[1]British Antarctic Survey, Cambridge, UK.

[2]División Glaciología, Instituto Antártico Argentino, Buenos Aires, Argentina.

It is argued that Larsen Ice Shelf contains marine ice formed by oceanic freezing and other mechanisms. Missing basal returns in airborne radar soundings and observations of a smooth and healed surface coincide downstream of regions where an ocean model predicts freezing. Visible imagery suggests that marine ice currently stabilizes Larsen C Ice Shelf and implicates failure of marine flow bands in the 2002 Larsen B Ice Shelf collapse. Ocean modeling indicates that any regime change towards the incursion of warmer Modified Weddell Deep Water into the Larsen C cavity could curtail basal freezing and its stabilizing influence.

1. Introduction

Ice shelves around the Antarctic Peninsula (AP) have shown progressive and ongoing retreat in recent decades that is widely believed to be associated with rapid atmospheric warming [*Vaughan and Doake*, 1996]. West of the AP, air and ocean temperatures are relatively high and few ice-shelf fragments remain, while on the eastern side both are lower and much of Larsen Ice Shelf (LIS) is still present. However, collapses of Larsen A Ice Shelf in 1995 and Larsen B Ice Shelf (LBIS) in 2002 have led to concern over the stability of the larger Larsen C Ice Shelf (LCIS). Such collapses have little direct effect on sea level, but the accompanying reduced buttressing of inshore glaciers led to increased ice discharge and sea-level rise [*Rignot et al.*, 2004].

In addition to atmospheric effects, it is argued that LIS has been thinned by increased ocean melting [*Shepherd et al.*, 2003], possibly linked to Weddell Deep Water (WDW) warming in recovery from the 1970s Weddell Polynya [*Robertson et al.*, 2002]. *Nicholls et al.* [2004] observed Modified Weddell Deep Water (MWDW) and Ice Shelf Water (ISW; below the surface freezing point and thus laced with ice-shelf meltwater) at the northern end of LCIS and deduced that the ISW was derived from MWDW cooled to the surface freezing point by interaction with the atmosphere. If waters flushing LCIS cavity are universally constrained to the surface freezing point, WDW warming could not thin LCIS.

The ocean may freeze onto ice shelves as well as melting them, and there is reason to expect that this occurs beneath LIS. Water at the surface freezing point melts ice shelves because the freezing temperature decreases with pressure, and resulting meltwater generates a thermohaline circulation in which cold, buoyant, ascending currents may become supercooled and form marine ice on the base of the ice shelf [*Robin*, 1979]. Other processes can also form marine ice [*Vaughan et al.*, 1993; *Rignot and MacAyeal*, 1998]. We utilized airborne radio-echo sounding (RES) data, satellite visible imagery, and an ocean model to assess the evidence for, and effect of, marine ice in LIS.

2. Survey data

We analyzed data from the 1997–1998 British Antarctic Survey–Instituto Antártico Argentino airborne RES survey ('9798' data), seeking evidence of marine ice and ice drafts for the ocean model. The survey used differential GPS and a radar transmitting a conventional 0.25-μs pulse around 150 MHz. Missions were flown with a nominal 150-m terrain clearance and ice thickness was derived using an 168-m μs^{-1} wave-velocity and 10-m firn correction. Position was determined to < 0.5 m and crossover analysis yielded RMS differences of 12 m ice thickness and 4 m elevation.

Figure 1 shows near-continuous 9798 RES surface returns, but basal returns are missing in open rifts and (shaded) flow bands in the wake of promontories and islands; we hypothesize that marine ice causes the latter. Marine ice basal returns are rarely detectable because it has high dielectric absorption [*Thyssen*, 1988] and can form an unconsolidated, diffuse base [*Engelhardt and Determann*, 1987]. Meteoric–marine ice interfaces are more commonly detected, but no such signal occurs in the 9798 data, perhaps because the radar was optimized for thicker ice. Thus, we could not derive marine ice thickness from isostatic anomaly (e.g. *Fricker et al.* [2001], who also had some missing returns over marine ice).

In LCIS, visible imagery supports a marine origin of these flow bands (Figure 1). First, they are smooth when, situated between glacier flow units, they might be heavily crevassed by shear. Second, other flow units contain rifts whose lateral propagation is clearly limited by the marine bands; this process governs iceberg-calving and ice-front geometry. There are several reasons why such behavior implies marine ice: oceanic freezing increases mean ice-shelf temperature and thus decreases its viscosity [*Larour et al.*, 2005]; ice's critical crevassing strain-rate decreases with temperature [*Vaughan*, 1993], so warm marine ice will increasingly deform rather than fail in response to stress; and marine ice heals rifts, binding their edges together with deformable material [*Rignot and MacAyeal*, 1998].

Ice draft (Figure 2) was obtained by combining 9798 basal elevations with older BEDMAP ice thicknesses [*Lythe et al.*, 2001] using a 9798 thickness–elevation relation (also used to fill missing basal returns). Latitude-dependence improved the relation (significance level $\ll 1$ %), so we used $h = -274.5 + 0.10D - 4.22\phi$, where h, D, and ϕ are surface elevation, ice thickness, and latitude. We attribute the northward-decreasing intercept in this relation to firn compaction as a result of higher air temperatures [*Vaughan and Doake*, 1996]. If this spatial correlation implies a temporal firn depth–temperature linkage, recent warming may have caused firn compaction that contributed to LIS surface lowering [*Shepherd et al.*, 2003]. Drafts outside our area of interest were filled using the 9798 relation and an elevation dataset [*Liu et al.*, 2001] and the final data were adjusted to the EIGEN-GL04C geoid [*Förste et al.*, 2008] and smoothed for model stability [*Holland and Feltham*, 2006]. The eastern boundary approximately follows the LCIS ice front, including most of LBIS and easing the implementation of model boundary conditions.

Inferred marine bands emanate from 'source' regions thinned by ice flow divergence from stagnant promontories (Figure 2). This provides at least three candidate formation mechanisms, producing different types of marine ice that we cannot differentiate: a) 'sea ice', formation of saline ice mélange in rifts. This grows at the rate of landfast sea ice with additional basal freezing [*Khazendar and Jenkins*, 2003] and occurs in rifted source regions in LBIS [*Glasser and Scambos*, 2008] that are absent in LCIS (Figure 1). b) 'flooding', seawater infiltration of firn. Wilkins Ice Shelf firn floods when it is depressed below sea level before pore close-off [*Vaughan et al.*, 1993], probably generating marine ice at the surface accumulation rate. LIS sources are similar: near-stagnant ice, 100–200 m thick, with 10–50 cm a^{-1} water-equivalent accumulation [*Turner et al.*, 2002]. c) 'oceanic' basal freezing. Ice-shelf basal melting commonly peaks near deep-drafted glacier inflows, and rising buoyant meltwater may supercool due to its increasing in-situ freezing temperature [*Robin*, 1979], freezing onto the ice base and growing and depositing frazil ice crystals. However, Coriolis force causes meltwater to flow geostrophically across-slope, so the primary constraints forcing it to ascend and supercool are grounded-ice barriers perpendicular to draft contours [*Holland and Feltham*, 2006]. Therefore, in general the most favorable oceanic freezing locations are the marine ice sources observed here, basal 'hollows' (ice-draft minima) downstream of deep inflows bounded to the left by grounded ice [e.g *Fricker et al.*, 2001]. Oceanic freezing rates vary depending upon local conditions, so we modeled ocean properties to assess freezing beneath LIS.

3. Model

A two-dimensional (depth-averaged) plume model [*Holland and Feltham*, 2006] was used to investigate LIS, representing buoyancy-driven meltwater flow but neglecting other important processes such as tides and water-column thickness variations. The model represents marine ice accretion in detail, simulating direct basal melting and freezing and the growth and deposition of frazil ice over 10 size classes. At 1-km resolution (10-s timestep), it resolves draft features and frazil dynamics relatively well.

Plume parameters used by *Payne et al.* [2007] and frazil settings of *Holland et al.* [2007] were unchanged except for the entrainment coefficient (see below) and latitude 67°S. The plume evolves to steady state from fixed-property inflow regions [*Payne et al.*, 2007] placed wherever draft exceeds 1000 m (400 m) beneath LCIS (LBIS). A uniform ambient ocean surrounds the active plume. From the observed LCIS outflow and simple theory, *Nicholls et al.* [2004] infer that the cavity contains MWDW at surface freezing temperature, so our basic 'cool' case used an ambient with potential temperature -1.9 °C, salinity 34.65. We also ran an extreme 'warm' case at -1.4 °C, 34.57, properties of the warmest MWDW adjacent to LIS [*Nicholls et al.*, 2004].

After 240 days, the steady cool-case results feature a thick meltwater layer sourced in rapidly-melting deep regions near the grounding line and flowing geostrophically along draft contours (Figure 3a). The plume thickens in basal hollows because meltwater fills them before spilling upwards over their sides. Under LCIS, meltwater from the whole grounding line combines into a central plume that flows along-slope until it is deflected out of the cavity by Jason Peninsula. This current reflects the entire LCIS system, so we tuned the entrainment coefficient to match observations of its $\approx$ 200-m thick outflow with potential temperature -2.1 °C, salinity 34.55 [*Nicholls et al.*, 2004]. Melt and freeze patterns were insensitive to this parameter, whose final value of 2×10^{-3} is within the range tested previously [*Holland and Feltham*, 2006; *Payne et al.*, 2007].

Generally weak melting (Figure 3b) peaks below deep glaciers, which have steep bases (hence rapid currents and high turbulent heat flux) and large thermal driving (freezing temperature decreases with depth). Marine ice accumulates in the larger hollows named in Figure 1, suggesting that oceanic freezing is a primary source of marine ice advected downstream by the ice. Meltwater is constrained to ascend into these hollows (and supercool) by grounded ice to its left. Vigorous frazil deposition causes high accumulation near Churchill Peninsula, in agreement with the broad marine band in Figure 1, which arises from the confluence of the central geostrophic plume and boundary-trapped meltwater from the south.

Predicted LBIS freezing agrees with Figure 1, but the applicability to LBIS of the ambient ocean forcing is uncertain and its marine ice could be entirely mélange. Oceanic freezing might contribute marine ice to the LCIS rifts near Jason and Kenyon peninsulas but their processes are inaccurately modeled here. Elsewhere beneath LCIS, freezing rates are apparently comparable to flooding ($<$ 0.2 m a^{-1}), apart from near Churchill Peninsula, but this is probably an underestimation. In general application the model predicts direct freezing (order 0.1 m a^{-1}), wherever the ice base is supercooled, surrounding focused frazil deposition (order 1 m a^{-1}), where the plume is depth-average supercooled; the latter is a smaller area because the freezing temperature decreases with depth [*Holland and Feltham*, 2006]. The plume is depth-average supercooled only off Churchill Peninsula, so other regions experience only direct freezing; part of the plume is supercooled and should grow frazil, but our depth-averaged model cannot resolve this. Three-dimensional models require considerable resources to run at frazil-resolving temporal and spatial resolution, and despite its simplicity our model demonstrates consistency between freezing locations and observed ocean conditions.

In the warm case (temperature increased by 0.5 °C) melting remains generally weak (Figure 3c), but high melting near grounding lines increases in extent and rate. Freezing halts everywhere apart from Churchill Peninsula, where a reduction occurs as frazil deposition ceases. Freezing is bolstered south of Jason Peninsula by increased volumes of meltwater from upstream. Cool and warm cases have mean LIS melt rates of 0.27 m a^{-1} (15.1 Gt a^{-1}) and 1.26 m a^{-1} (69.5 Gt a^{-1}) respectively, revealing a low sensitivity to temperature change (2 m a^{-1} °C^{-1}) that fits the theory that ice shelves forced by cooler waters are less susceptible to warming [*Holland et al.*, 2008]. Melt rates reflect our idealized model and are not best estimates; *Rignot et al.* [2008] estimate that the northern AP discharged 20 ± 3 and 49 ± 3 Gt a^{-1} in 1996 and 2006 respectively.

4. Discussion

It is informative to consider earlier studies of LBIS, which inferred weak ice downstream of Foyn Point and Cape Disappointment [*Vieli et al.*, 2006; *Khazendar et al.*, 2007]. These were rifted 'suture zones', and their weakening could have contributed to LBIS collapse [*Glasser and Scambos*, 2008]. Ice mélange formed in these rifts comprised the marine ice that we observe downstream, confirming earlier speculation [*Khazendar et al.*, 2007]. Rifts lessened downstream, suggesting that they were absent in the past [*Glasser and Scambos*, 2008] or are healed by compression [*Vieli et al.*, 2006]; we suggest that our inferred marine bands and modeled freezing are also consistent with healing by marine ice. It is possible that climatic change reduced marine ice formation, weakening sutures between flow units and contributing to LBIS collapse. Beneath LCIS, marine ice limits rifts and appears to bind flow units together, so an understanding of its effect is necessary to assess the future of LIS. Marine-ice mechanisms could stabilize ice shelves in the cool waters east of the AP, but will be reduced in warmer conditions to its west.

Sea-ice formation in rifts will respond to changes in almost any climatic variable, while marine ice formation by flooding would be affected by the increasing accumulation near LIS [*Thomas et al.*, 2008]. Oceanic freezing will reduce if warmer waters access the cavity, providing a link between LCIS stability and Weddell Sea conditions that is more complex than a simple melting–temperature relationship. Our model suggests that the outflow observed by *Nicholls et al.* [2004] derives from the whole ice shelf, so their deduction that cool MWDW drives melting, rather than warming WDW, applies universally rather than just in the vicinity of their measurements. All cavity waters are therefore sourced at the surface freezing temperature, so a warming would require either weaker modification of the MWDW entering the cavity (reduced continental-shelf sea ice formation) or an increased supply of warm off-shelf MWDW (changed ocean circulation). Wind-forced changes of the latter type are thought to affect ice shelves in the Amundsen Sea [*Thoma et al.*, 2008]. The pattern of LIS elevation change attributed to increased basal melting [*Shepherd et al.*, 2003] apparently requires warming focused on the north of the cavity rather than the uniform warming modeled here.

5. Conclusions

Airborne RES data, satellite visible imagery, and a simple ocean model lead us to the following conclusions:

1. LIS contains flow bands comprised of marine ice, which is advected downstream by ice flow after forming in thin areas between glacier flow units in the immediate wake of peninsulas. This is consistent with previously inferred LBIS rheologies.

2. Different types of marine ice, which we cannot distinguish, could be formed by ocean freezing, sea ice formation in rifts, and seawater-flooded firn. The model indicates that rising meltwater causes significant oceanic freezing beneath LIS. Visible imagery suggests that sea-ice formation in rifts occurred only in LBIS at the time of survey. Flooding could generate marine ice at the surface accumulation rate and cannot be ruled out.

3. Marine ice laterally limits rifts formed in LCIS meteoric flow units and thereby controls iceberg calving and ice-front geometry. Warm marine ice has a low viscosity and can deform rapidly without fracturing, and oceanic freezing heals rifted meteoric ice. Marine ice could thus reduce the likelihood of LCIS collapse. Failure of marine bands was implicated in the LBIS collapse.

4. A LCIS cavity filled with warmer water would experience greater melting and less-widespread freezing. The model suggests that MWDW melts LCIS, so such a change could arise through reduced cooling of MWDW over the continental shelf or an increased supply of warmer MWDW onto the shelf. The observed WDW warming probably cannot affect LCIS.

In-situ survey, ice-coring, and improved ocean modeling and observation are now necessary to confirm the origin and properties of LIS marine ice.

References

ADD Consortium (2002), Antarctic Digital Database, SCAR, Cambridge, http://www.add.scar.org/.

Engelhardt, H., and J. Determann (1987), Borehole evidence for a thick layer of basal ice in the central Ronne Ice Shelf, *Nature*, *327*, 318–319.

Förste, C., et al. (2008), The GeoForschungsZentrum Potsdam/Groupe de Recherche de Geodesie Spatiale satellite-only and combined gravity field models: EIGEN-GL04S1 and EIGEN-GL04C, *J. Geod.*, *82*, 331346, doi:10.1007/s00190-007-0183-8.

Fricker, H. A., S. Popov, I. Allison, and N. Young (2001), Distribution of marine ice beneath the Amery Ice Shelf, *Geophys. Res. Lett.*, *28*, 2241–2244.

Glasser, N. F., and T. A. Scambos (2008), A structural glaciological analysis of the 2002 Larsen B Ice Shelf collapse, *J. Glaciol.*, *54*, 3–16.

Holland, P. R., and D. L. Feltham (2006), The effects of rotation and ice shelf topography on frazil-laden Ice Shelf Water plumes, *J. Phys. Oceanogr.*, *36*, 2312–2327.

Holland, P. R., D. L. Feltham, and A. Jenkins (2007), Ice Shelf Water plume flow beneath Filchner-Ronne Ice Shelf, Antarctica, *J. Geophys. Res.*, *112*, C05044, doi:10.1029/2006JC003915.

Holland, P. R., A. Jenkins, and D. M. Holland (2008), The response of ice shelf basal melting to variations in ocean temperature, *J. Clim.*, *21*, 2558–2572.

Khazendar, A., and A. Jenkins (2003), A model of marine ice formation within Antarctic ice shelf rifts, *J. Geophys. Res.*, *108*, 3235–3248.

Khazendar, A., E. Rignot, and E. Larour (2007), Larsen B Ice Shelf rheology preceding its disintegration inferred by a control method, *Geophys. Res. Lett.*, *34*, L19503, doi:10.1029/2007GL030980.

Larour, E., E. Rignot, I. Joughin, and D. Aubry (2005), Rheology of the Ronne Ice Shelf, Antarctica, inferred from satellite radar interferometry data using an inverse control method, *Geophys. Res. Lett.*, *32*, L05503, doi:10.1029/2004GL021693.

Liu, H., K. Jezek, B. Li, and Z. Zhao (2001), RAMP digital elevation model, NSIDC, Boulder, http://www.nsidc.org/.

Lythe, M. B., D. G. Vaughan, and the BEDMAP Consortium (2001), BEDMAP: a new ice thickness and subglacial topographic model of Antarctica, *J. Geophys. Res.*, *106*, 11 335–11 351.

Nicholls, K. W., C. J. Pudsey, and P. Morris (2004), Summertime water masses off the northern Larsen C Ice Shelf, Antarctica, *Geophys. Res. Lett.*, *31*, L09309, doi:10.1029/2004GL019924.

Payne, A. J., P. R. Holland, A. P. Shepherd, I. C. Rutt, A. Jenkins, and I. Joughin (2007), Numerical modelling of ocean–ice interactions under Pine Island Bay's ice shelf, *J. Geophys. Res.*, *112*, C10019, doi:10.1029/2006JC003733.

Rignot, E., and D. R. MacAyeal (1998), Ice-shelf dynamics near the front of the Filchner-Ronne Ice Shelf, Antarctica, revealed by SAR interferometry, *J. Glaciol.*, *44*, 405–418.

Rignot, E., G. Casassa, P. Gogineni, A. Rivera, and R. Thomas (2004), Accelerated ice discharge from the Antarctic Peninsula following the collapse of Larsen B Ice Shelf, *Geophys. Res. Lett.*, *31*, L18401, doi:10.1029/2004GL020697.

Rignot, E., J. L. Bamber, M. R. van den Broeke, C. Davis, Y. Li, W. J. van de Berg, and E. van Meijgaard (2008), Recent Antarctic ice mass loss from radar interferometry and regional climate modelling, *Nature Geoscience*, *1*, 106–110, doi:10.1038/ngeo102.

Robertson, R., M. Visbeck, A. L. Gordon, and E. Fahrbach (2002), Long-term temperature trends in the deep waters of the Weddell Sea, *Deep-Sea Res. II*, *49*, 4791–4806.

Robin, G. de Q. (1979), Formation, flow and disintegration of ice shelves, *J. Glaciol*, *24*, 259–271.

Scambos, T. A., T. M. Haran, M. A. Fahnestock, T. H. Painter, and J. Bohlander (2007), MODIS-based Mosaic of Antarctica data sets: Continent-wide surface morphology and snow grain size, *Remote Sens. Environ.*, *111*, 242–257.

Shepherd, A. P., D. J. Wingham, A. J. Payne, and P. Skvarca (2003), Larsen Ice Shelf has progressively thinned, *Science*, *302*, 856–859.

Sievers, J., A. Grindel, and W. Meier (1989), Digital satellite image mapping of Antarctica, *Polarforschung*, *59*, 25–33.

Thoma, M., A. Jenkins, D. Holland, and S. Jacobs (2008), Modelling Circumpolar Deep Water intrusions on the Amundsen Sea continental shelf, Antarctica, *Geophys. Res. Lett.*, *35*, L18602, doi:10.1029/2008GL034939.

Thomas, E. R., G. J. Marshall, and J. R. McConnell (2008), A doubling in snow accumulation in the western Antarctic Peninsula since 1850, *Geophys. Res. Lett.*, *35*, L01706, doi:10.1029/2007GL032529.

Thyssen, F. (1988), Special aspects of the central part of Filchner-Ronne Ice Shelf, Antarctica, *Ann. Glaciol.*, *11*, 173–179.

Turner, J., T. A. Lachlan-Cope, G. J. Marshall, E. M. Morris, R. Mulvaney, and W. Winter (2002), Spatial variability of Antarctic Peninsula net surface mass balance, *J. Geophys. Res.*, *107*, D134173, doi:10.1029/2001JD000755.

Vaughan, D. G. (1993), Relating the occurrence of crevasses to surface strain rates, *J. Glaciol.*, *39*, 255–266.

Vaughan, D. G., and C. S. M. Doake (1996), Recent atmospheric warming and retreat of ice shelves on the Antarctic Peninsula, *Nature*, *379*, 328–331.

Vaughan, D. G., D. R. Mantripp, J. Sievers, and C. S. M. Doake (1993), A synthesis of remote sensing data on Wilkins Ice Shelf, Antarctica, *Ann. Glaciol.*, *17*, 211–218.

Vieli, A., A. J. Payne, Z. Du, and A. Shepherd (2006), Numerical modelling and data assimilation of the Larsen B Ice Shelf, Antarctic Peninsula, *Philos. Trans. R. Soc. Ser. A*, *364*, 1815–1839.

Figure 1. (a) 1986 Landsat image of LBIS [*Sievers et al.*, 1989] and (b) 2003-2004 MOA image of LCIS [*Scambos et al.*, 2007], both with 9798 survey data. Red and (overlain) blue points mark surface and basal returns, so visible red points indicate failure to detect the base. Yellow shading indicates proposed marine ice and yellow tracks are other surveys incorporated in the ice draft. The star indicates *Nicholls et al.* [2004] ocean observations. Major islands and peninsulas are named.

Figure 2. Derived ice draft (contoured within the model domain) and 1992 ice front [*ADD Consortium*, 2002].

Figure 3. (a) Cool case plume thickness (colored) and velocities (every fourth grid point). (b) Direct basal melt/freeze plus frazil precipition in cool case (colored; m a^{-1} ice; melting is positive) and ice shelf draft (gray, 100–500 m in 25-m steps). (c) same as (b) for warm case.

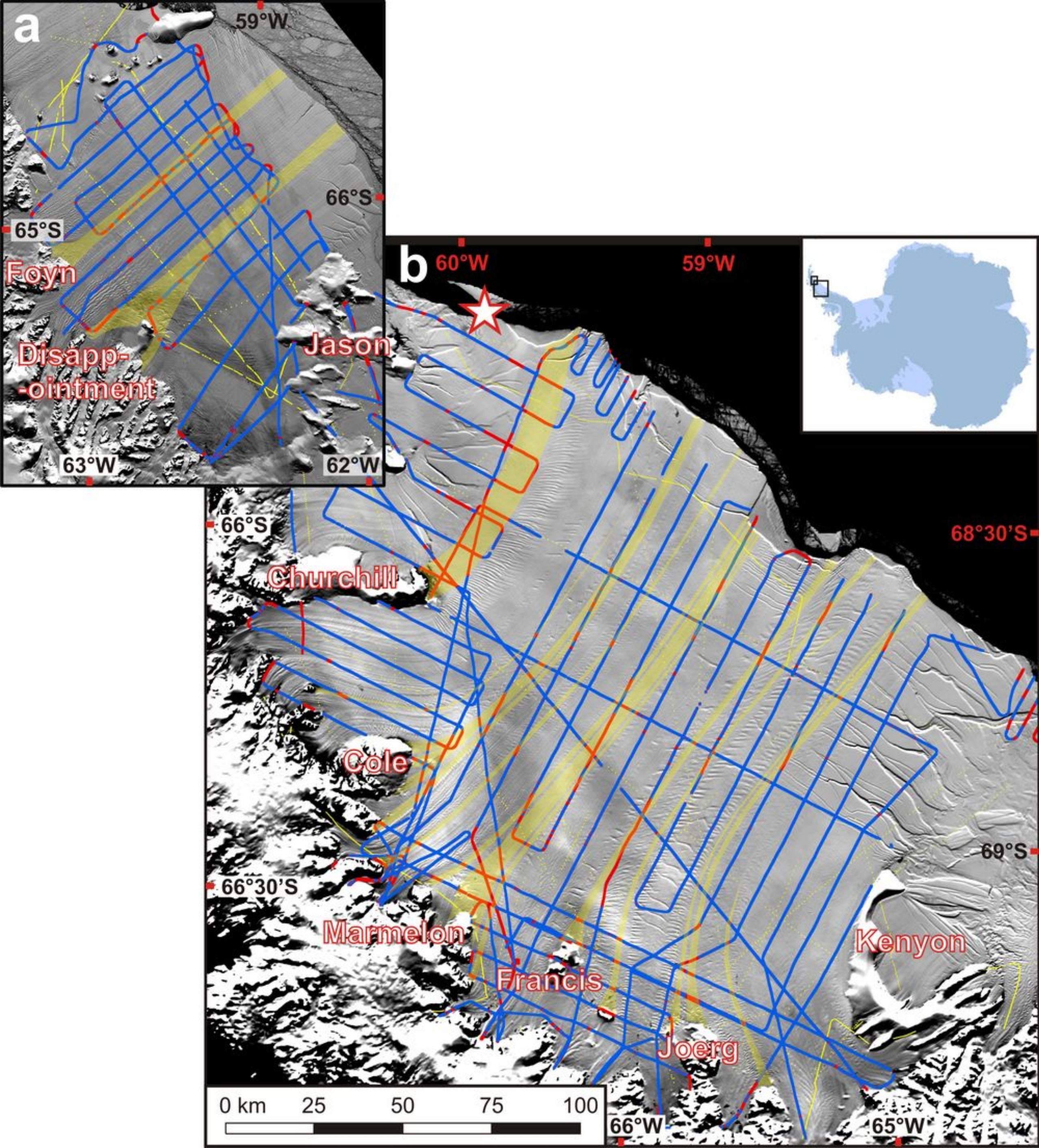

a
59°W
66°S
65°S
Foyn
Disapp-
-ointment
Jason
63°W
62°W
b
60°W
59°W
66°S
68°30'S
Churchill
Cole
69°S
66°30'S
Marmelon
Francis
Kenyon
Joerg
0 km
25
50
75
100
66°W
65°W

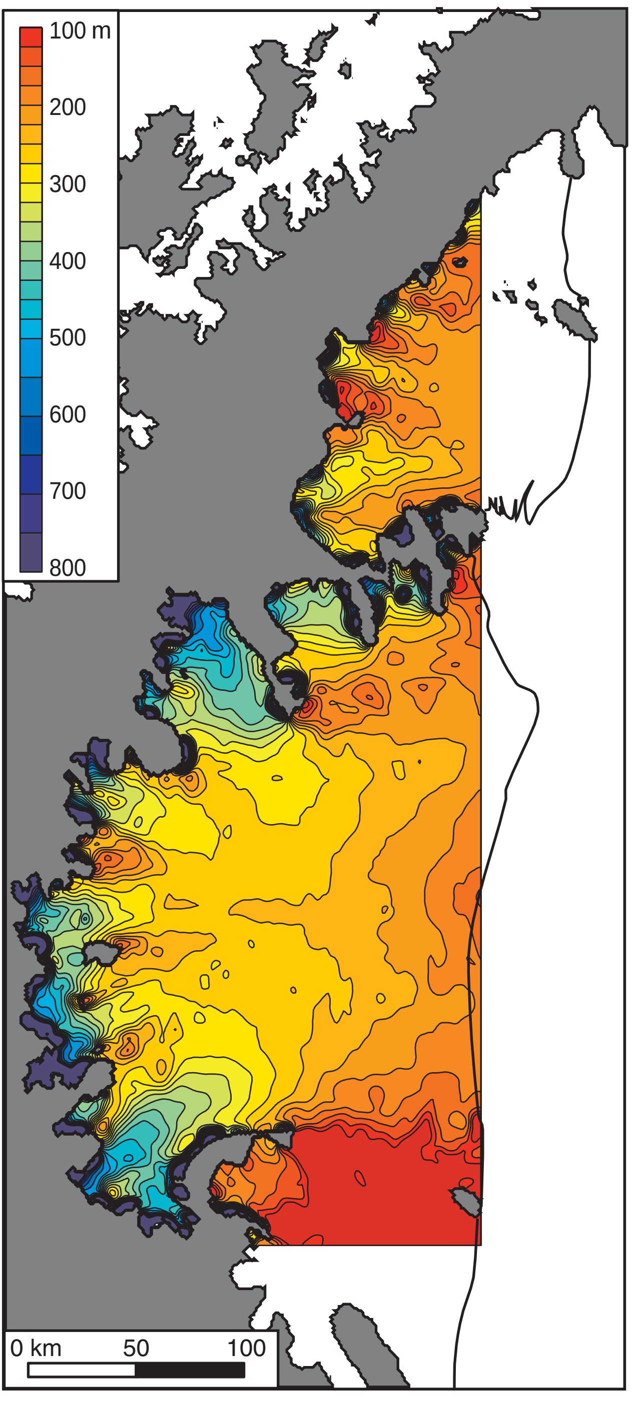

100 m
200
300
400
500
600
700
800
0 km
50
100

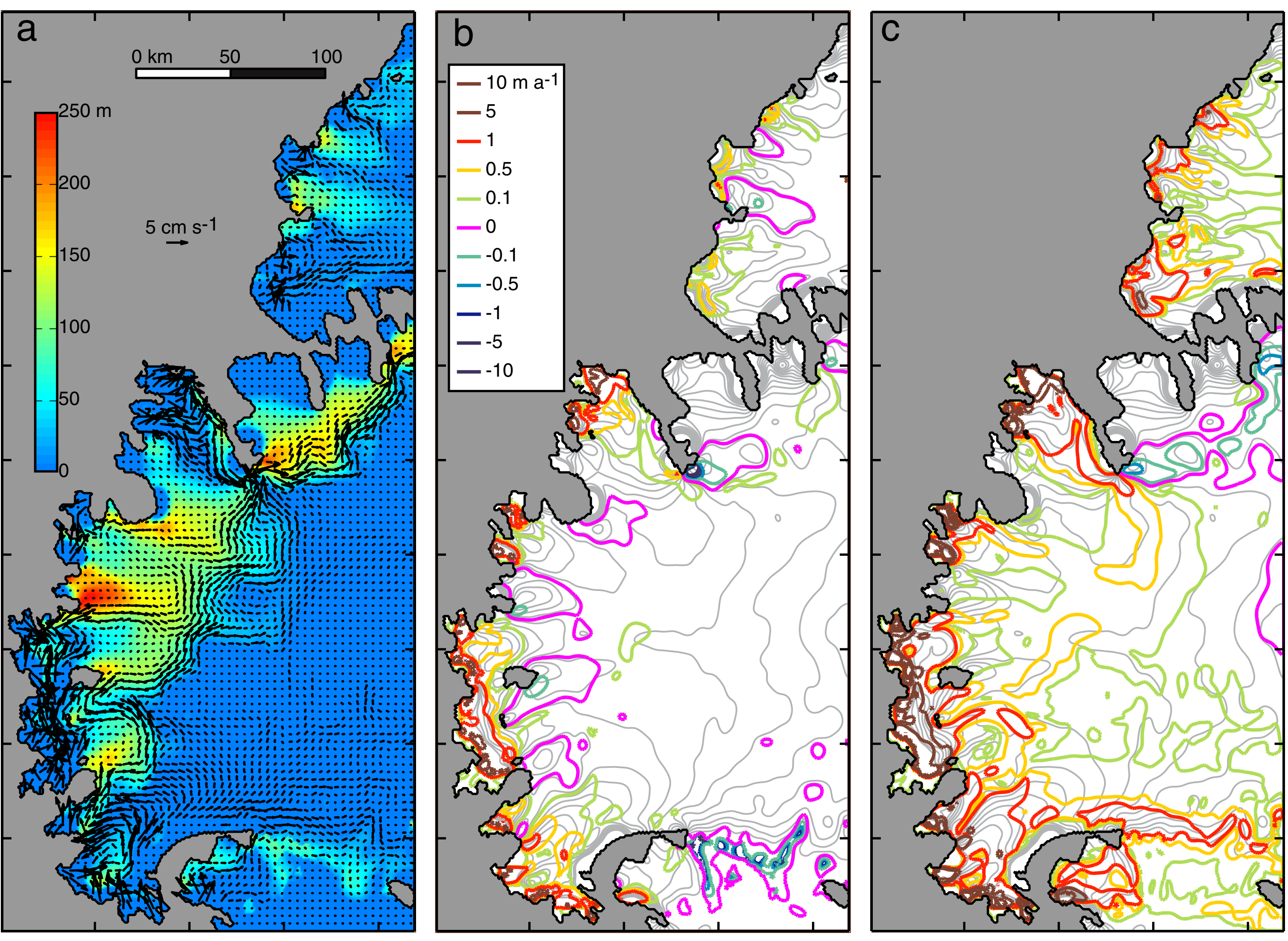
a
0 km
50
100
250 m
200
150
100
50
0
5 cm s-1
b
10 m a-1
5
1
0.5
0.1
0
-0.1
-0.5
-1
-5
-10
c